

Full Poincaré polarimetry enabled through physical inference

CHAO HE,^{1,*} JIANYU LIN,^{2,3} JINTAO CHANG,⁴ JACOPO ANTONELLO,¹ BEN DAI,⁵ JINGYU WANG,¹ JIAHE CUI,¹ JI QI,^{2,3} MIN WU,⁶ DANIEL S. ELSON,^{2,3} PENG XI,⁷ ANDREW FORBES,⁸ AND MARTIN J. BOOTH^{1,9}

¹Department of Engineering Science, University of Oxford, Parks Road, Oxford OX1 3PJ, UK

²Hamlyn Centre for Robotic Surgery, Imperial College London, London SW7 2AZ, UK

³Department of Surgery and Cancer, Imperial College London, London SW7 2AZ, UK

⁴Department of Physics, Tsinghua University, Beijing 100084, China

⁵Department of Statistics, The Chinese University of Hong Kong, Shatin, HK SAR, China

⁶Department of Computer Science, University of Oxford, Parks Road, Oxford OX1 3QD, UK

⁷Department of Biomedical Engineering, College of Engineering, Peking University, Beijing 100871, China

⁸School of Physics, University of the Witwatersrand, Private Bag 3, Johannesburg 2050, South Africa

⁹e-mail: martin.booth@eng.ox.ac.uk

*Corresponding author: chao.he@eng.ox.ac.uk

Received 3 January 2022; revised 27 August 2022; accepted 29 August 2022; published 23 September 2022

While polarization sensing is vital in many areas of research, with applications spanning from microscopy to aerospace, traditional approaches are limited by method-related error amplification, accumulation, and pre-processing steps, constraining the performance of single-shot polarimetry. Here, we propose a measurement paradigm that circumvents these limitations, based on the use of a universal full Poincaré generator to map all polarization analyzer states into a single vectorially structured light field. All vector components are analyzed in a single shot, extracting the vectorial state through inference from a physical model of the resulting image, providing a single-step sensing procedure. To demonstrate the feasibility of our approach, we use a common graded index (GRIN) optic as our mapping device and show mean errors of <1% for each vector component. Our work paves the way for next-generation polarimetry, impacting a wide variety of applications that rely on vector measurement.

Published by Optica Publishing Group under the terms of the [Creative Commons Attribution 4.0 License](https://creativecommons.org/licenses/by/4.0/). Further distribution of this work must maintain attribution to the author(s) and the published article's title, journal citation, and DOI.

<https://doi.org/10.1364/OPTICA.452646>

1. INTRODUCTION

Polarization sensing methods have wide applications which range from quantum physics to clinical applications [1–19]. They can be divided into two categories: time-resolved, where measurements are taken using a sequence of analyzers in a time-multiplexed manner, or single-shot, where different analyzers are spatially multiplexed. Time-resolved measurements can be easier to implement, but single-shot methods are crucial for applications with rapidly changing inputs or where high throughput is required. Single-shot polarimetry based on passive devices features advantages such as high stability compared with active counterparts. The standard measurement approaches in both methods are directly or indirectly related to a core measurement equation [20–24]: $S = \text{inv}(A) \cdot I$, where S is the Stokes vector to be measured, and I is the vector of intensities recorded at the detector. Matrix A is known as the instrument matrix, which is determined by the system configuration. In order to enhance precision and accuracy, numerous attempts have been made to push A toward an optimal matrix as it determines the properties of the error propagation

and hence affects the performance [20–24]. An evaluation of systematic error amplification level can be performed using the condition number (CN) of A , with the theoretical minimum value [20–24] $\text{CN} = \sqrt{3}$. In practice, traditional approaches require various processes to be implemented before the matrix calculation, which includes denoising, optimization, and calibration [20–33]. Although the detailed operating procedures are different among various polarimetry techniques, the complex error transfer and accumulation processes are fairly consistent [20–33] as all they essentially measure the vector property of the light beam in cumbersome and indirect ways. These place fundamental limits on precision and accuracy in single-shot polarimetry.

Here, we put forward a new paradigm that allows a single-shot polarimetry circumventing the error amplification factor and the necessary pre-processing steps. At the heart of our approach is the notion of full Poincaré beam (FPB) mapping, producing a particular form of vectorially structured light. The concept of a “full Poincaré beam” has been of great interest in optics for many years [34–39]. This interest stems from the uniqueness of the beam property, namely that the state of polarization (SOP) of the

beam's transverse cross section can cover the full Poincaré sphere, hence the name—FPB. Such beams are important for various applications utilizing structured light, such as singularity analysis and beam shaping [34–39], and they have been harnessed in a wide range of polarimetric measurement techniques [40–48]. However, in existing FPB polarimetry, the error amplification and accumulation processes are still present, as these methods are based on traditional matrix-based Stokes vector retrieval [31]. We harness a special class of the devices that can generate a FPB to enable our new paradigm, which we term a universal full Poincaré generator (UFGP). The essential feature here is the ability to generate different FPBs given different pure uniform incident SOPs (not all devices that can generate a FPB are also UFGPs; see Supplement 1, Note 1). The FPB generated via the UFGP provides all the information required to deduce the initial unknown SOP when mapped onto an intensity image through a polarization analyzer. We highlight here that the spatial variation in intensity provides a simple intuitive route to polarization measurement, as there is a unique link between the intensity pattern and the input SOP. This provides new prospects for direct vector sensing through use of image processing to retrieve the incident SOP, rather than using an indirect matrix-based method.

Figure 1 illustrates conceptually how the UFGP-based paradigm works, using a simple graded index (GRIN) lens system as an example UFGP (other implementation options are explained in Section 3). In this initial work, we focus on point measurements rather than imaging. A pinhole is used in our system in order to make sensing equivalent to a point measurement (see Supplement 1, Notes 1 and 2). We use an illumination beam with an arbitrarily chosen linear or elliptical SOP for demonstration purposes (in reality, this represents the unknown input state). A FPB is generated [Fig. 1(b)] after this passes through the GRIN lens [24,35]. The output vector field is then filtered via a polarization filter (PF) assembly (the right-hand circular SOP is selected as the eigenstate here) leading to a non-uniform intensity distribution [Fig. 1(b)] that can be recorded at the detector. Intuitively, one can understand that the brightest points within the intensity distribution must correspond to the eigenstate of the PF. The positions of these points depend upon the input state. Hence, the input SOP could—in principle—be read off directly from the positions of the brightest points, as long as the mapping of states to image position is known [see Fig. 1(c)]. As the GRIN lens is a UFGP of order two, there are two points of maximum intensity (see Supplement 1, Notes 1 and 2). The nature of this UFGP sensing paradigm means that we have access, in principle, to a complete set of all possible analyzer states in a single mapping. This goes beyond any other non-UFGP systems, as they cannot sense the “complete” set of states in the same way and hence cannot enable the same paradigm; and also goes beyond other matrix calculation-based UFGP polarimetry, as our paradigm retrieves the Stokes vector through physical inference from image analysis (see Supplement 1, Note 1). Our approach circumvents the above-mentioned mathematical limit, as here is no minimum error propagation amplification posed by the matrix process (see Supplement 1, Note 3). Instead, in theory its performance can be continuously boosted, even in a single shot, by judicious choice of detector pixel size and imaging optics, and in practice further enhanced by the use of intelligence in the imaging, such as through machine learning (ML).

Figure 1(d) provides a visualized example of the link between the incident SOPs [shown on the Poincaré sphere; Fig. 1(d), region

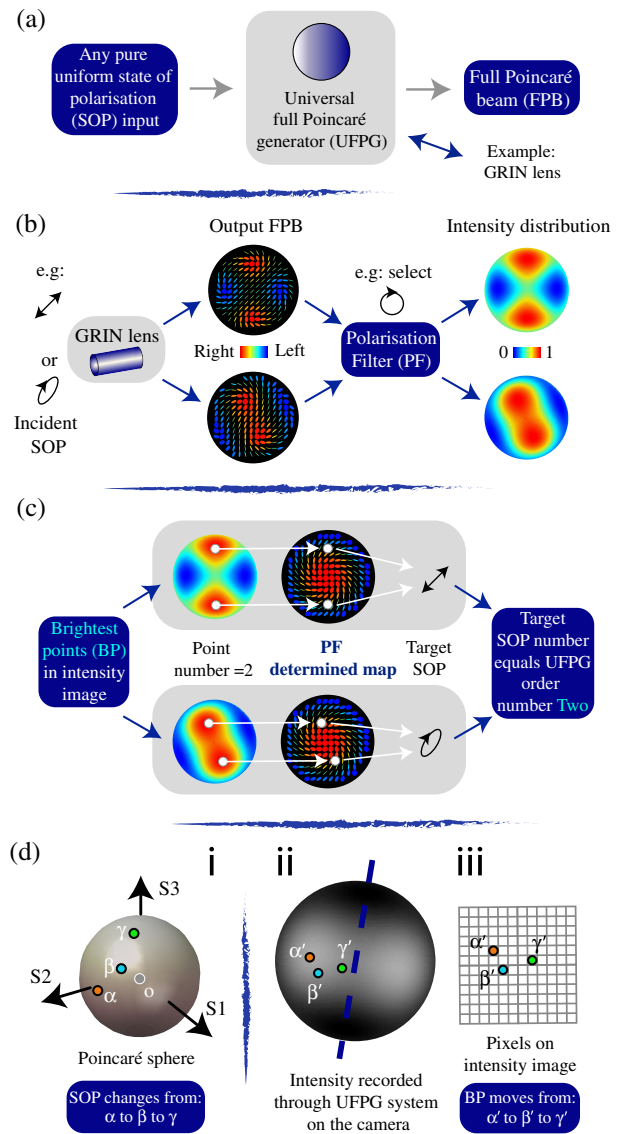


Fig. 1. Concepts and mechanisms of the UFGP paradigm. (a) Definition of a UFGP. (b) Intensity distribution generation process—including sending different incident SOPs through the GRIN lens system, obtaining corresponding output FPBs, and using a polarization filter (PF) to create an intensity image. (c) Intuitive explanation of the measurement process, illustrated through finding brightest points (BP) on the intensity distribution and reading the input SOP from the locations corresponding to these points on the PF determined FPB map. In practice, all points in the image feed into the estimation process. (d) Mapping of SOPs between domains. (i) Example SOPs (points α , β , γ) on the Poincaré sphere. (ii) The corresponding points α' , β' , γ' , mapped from points α , β , γ on the acquired intensity image. (iii) A sketch of the points as pixel positions recorded on the detector. The pixel size acts as a theoretical limit on the sensitivity of the new paradigm (see Supplement 1, Note 4).

(i)], the SOPs related locations mapped on the intensity image [Fig. 1(d), region (ii)], and a sketch of the pixel size on the detector [Fig. 1(d), region (iii)]. In order to determine the brightest point locations properly, the essential point of the new paradigm, we adopt a pure image-based sensing process (details in next section, and Supplement 1, Note 4). Instead of dividing the pipeline into denoising, optimization, and intensity and polarization calibration, we have managed to combine such processes in one step by remodeling the process into a combined fitting and estimation

task based upon image processing and machine-learning-enabled estimation of the brightest point. It is an optimal, system-based, integrated approach that enables high performance in precision, accuracy, and stability.

2. RESULTS

The feasibility of such a UFGP polarimeter was tested experimentally, with the results shown in Figs. 2 and 3. Effective realization of this method consists of two steps. First, fitting of a model to the intensity data is required in order to estimate the position of the brightest points. This needs to be robust against temporal or spatial noise [20–30]. Second, the mapping between the detected positions and the related SOP should be properly identified. To implement these image processing steps, we drew upon ML techniques [49–52], particularly through inspiration from the recent success of convolutional neural networks (CNNs) in computer vision [49–52]. Importantly, rather than treating the complex polarization measurement processes as separate steps as traditional methods have done [20–30], we implemented a single image-based “end-to-end” solution [51,52]. This way we avoid the need for separate procedures for denoising, optimization, and calibration (which can each introduce separate errors).

An overview of the sensing process is shown in Fig. 2(a). It consists of three steps: (1) build a system as a polarization state analyzer using a UFGP (see Supplement 1, Note 2 for details of the setup); (2) train a neural network based on a predetermined UFGP system with different intensity images (including different brightest point locations) featuring known SOPs (see Supplement 1, Note 4 for details of the “end-to-end” training); and (3) record the experimental intensity images of unknown SOPs, load them into the image processing framework to determine the original SOPs, and output the prediction (see details in Supplement 1, Note 4). The core of the image processing framework—the neural network—is illustrated in Fig. 2(b). An example of the input experimental

image, the constitution of the CNN, the output heatmap are also shown in the flow chart. Note here we use a widely used/validated non-polarization specific network [53] to solve the polarization measurement problem, based upon physical information. The rest of the framework [Fig. 2(c)] is an image post-processing procedure, which links the brightest point locations and the SOPs via a lookup table. For details refer to Supplement 1, Note 4. After such a process is established, the online sensing process requires only step 3 to be repeated.

Different SOPs along three selected curves (a total of 900 points) on the Poincaré sphere were tested to validate the feasibility and for error analysis. Both theoretical and experimental data are demonstrated in Fig. 3(a). Then 200 points were randomly sampled from the obtained data and the mean errors corresponding to elements of the Stokes vector: S_1 , S_2 , S_3 , Euclidean distance, and degrees of polarization (DOP) were calculated [Figs. 3(b) and 3(c)]. We achieve exceptional measurement precision across the Poincaré sphere with stable performance and robustness compared to existing techniques. Figure 3(d) and the Supplementary Tables also give a quantitative comparison with several established methods to demonstrate the outstanding precision and accuracy of the new paradigm. Our results also confirm the ability to differentiate small-scale polarization changes in a single shot with a sensitivity of ~ 0.01 (this is defined mathematically in relation to the UFGP system property and camera pixel number; see details in Supplement 1, Note 5), around 3 times better than the well-established traditional single-shot point Stokes polarimeter, and more than 6 times better than other modern approaches based on light–matter interactions, such as plasmonics, spin–orbit effects, and metasurfaces. In this work we mainly focus on fully polarized light detection and analysis. Detailed SOP retrieval under other conditions or with extra parameters such as DOP will form part of our future work.

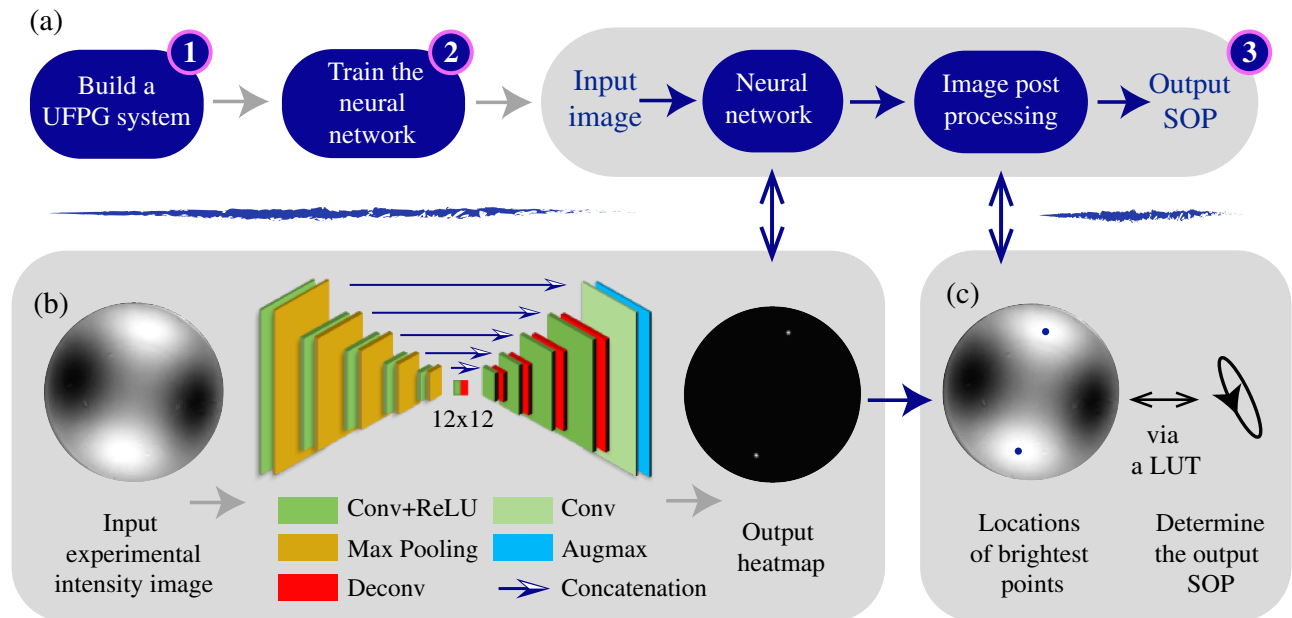


Fig. 2. Overview of the sensing process. (a) A flow chart of the ML-assisted UFGP-based paradigm that includes three steps. (b) and (c) show one practical exemplar of using the CNN-based image processing approach to retrieve the unknown incident SOP via an experimental intensity image. The neural network converts the input image to a mask featuring inferred positions of the brightest points (heatmap), while the image post-processing locates the brightest point locations and links to the output SOP via a LUT. Details are elaborated in Supplement 1, Note 4.

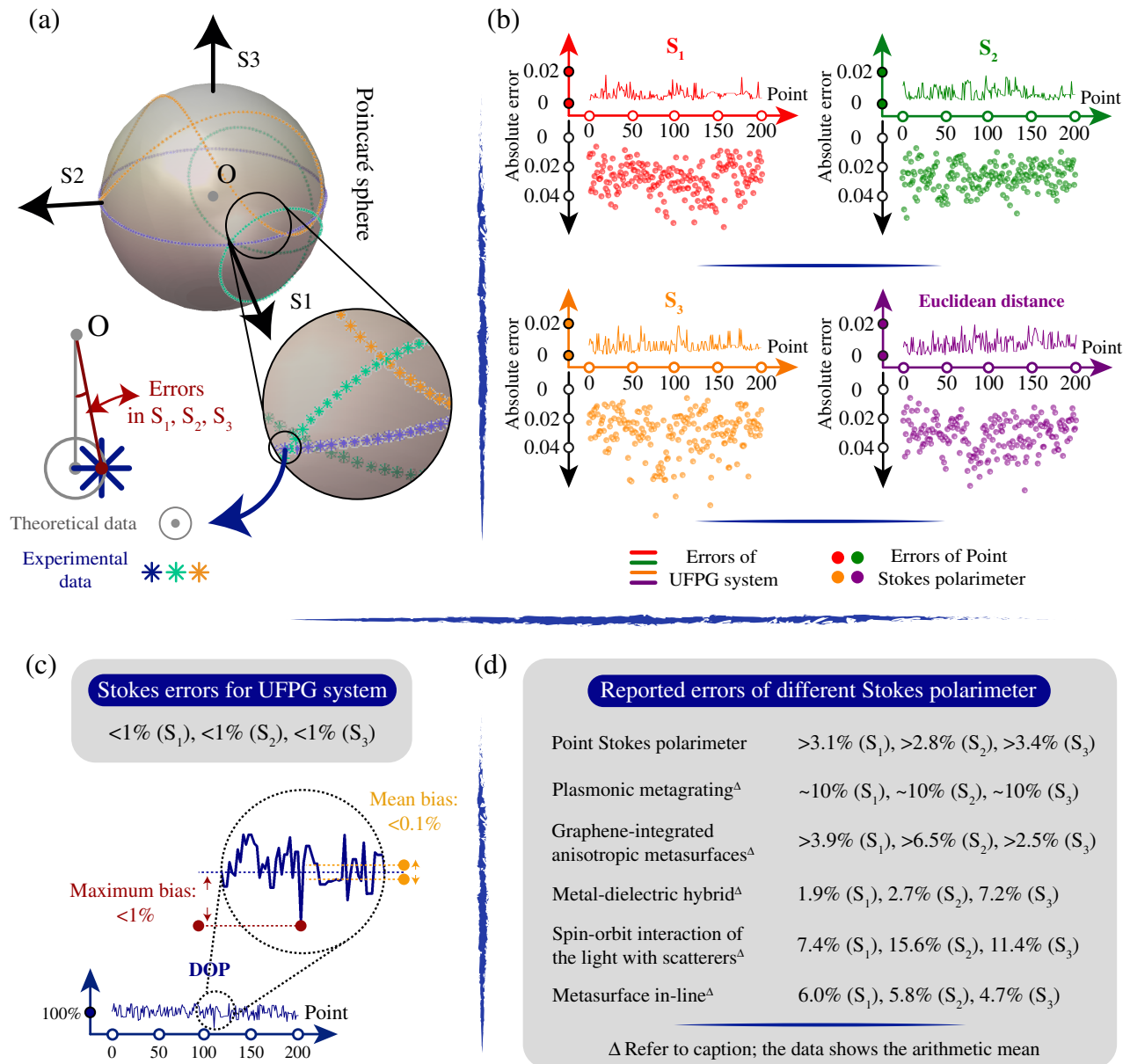


Fig. 3. Measurement performance verification of the UFGP paradigm, and comparison with recent reported techniques. (a) Three example curves (curves generated using an arbitrary state generator followed by a rotating quarter-wave plate; for details of the generator, see Supplement 1, Note 2) on the Poincaré sphere as a feasibility test for our new approach. Both theoretical and experimental data are presented on the sphere. Theoretical data are shown in gray circles; experimental counterparts are indicated by star symbols with different colors for different curves. The experimental setup is described in Supplement 1, Note 2. (b) Precision evaluation process. The error diagrams for S_1 , S_2 , S_3 , and Euclidean distance at 200 random points are acquired from the sampled curves on the Poincaré sphere. The same measurements were conducted by a traditional point Stokes polarimeter (i.e., a point measurement system; see Supplement 1, Note 5), whose measurement errors are plotted in colored ball symbols for an intuitive comparison. (c) The errors of Stokes vector components and parameter DOP of the UFGP system are presented with calculated magnitudes. (d) The reported error performance of several modern polarimeters [54]. Compared to those existing counterparts [54–58], our new approach demonstrates the exceptional measurement precision and accuracy (see more data in Supplement 1, Tables 1 and 2).

3. CONCLUSIONS AND DISCUSSION

In conclusion, we proposed a new paradigm for polarization sensing using a novel mapping of any input SOP to a structured light field with a physical optic, which is subsequently processed by a machine learning algorithm. It featured exceptional measurement precision and accuracy in single-shot operation with robust performance. In this paper, we used a GRIN lens as the UFGP because it is non-pixelated, produces high beam quality, is low cost, and is easily available [24]; however, the UFGP can

also take the form of a stressed optical element [33,47,48], digital micromirror device (DMD), spatial light modulator (SLM), metasurface, or an alternative device, as long as it is suitably configured. Further feasibility demonstrations are elaborated in Supplement 1, Notes 5 and 6, including for low intensity measurement, cases of various DOP, as well as an example of weak polarization error sensing. These validations show the solid performance of our new approach.

Future directions are available for further development of this concept. The sensitivity can be enhanced further by device substitution, as the fundamental minimum scale depends upon the number of pixels in the image (see [Supplement 1](#), Note 4). The use of UFGs with higher-order numbers could possibly lead to greater robustness and precision, linked to the enhancement of the pattern complexity [51,52]. The depolarization property can be readily extracted from the contrast of the intensity distribution image to reveal more polarimetric information (see [Supplement 1](#), Note 6). Furthermore, the UFG paradigm can be adapted to single-shot multi-point Stokes sensing (see [Supplement 1](#), Note 7). There are obviously still challenges to overcome for this technique to be applied in certain future applications (such as 3D sensing), but our work opens a unique avenue toward precise sensing of weak vectorial information, which will provide useful capability in any application that relies upon polarization sensing.

Funding. St. John's College, University of Oxford (Junior Research Fellowship (C.H.)); European Research Council (AdOMiS, No. 695140).

Acknowledgment. C. H. would like to express thanks for the support from the Junior Research Fellowship from St John's College, University of Oxford and thanks to Mr. Binguo Chen from Tsinghua University for the useful discussions.

Disclosures. The authors declare no competing interests.

Data availability. Data underlying the results presented in this paper are not publicly available at this time but may be obtained from the authors upon reasonable request.

Supplemental document. See [Supplement 1](#) for supporting content.

REFERENCES

1. R. Oldenbourg, "A new view on polarization microscopy," *Nature* **381**, 811–812 (1996).
2. R. A. Chipman, W.-S. T. Lam, and G. Young, *Polarized Light and Optical Systems* (CRC Press, 2018).
3. S. Cloude, *Polarisation: Applications in Remote Sensing* (Oxford University, 2009).
4. H. Rubinsztein-Dunlop, A. Forbes, M. Berry, M. Dennis, D. Andrews, M. Mansuripur, C. Denz, C. Alpmann, P. Banzer, T. Bauer, E. Karimi, L. Marrucci, M. Padgett, N. Litchinitser, N. Bigelow, C. Rosales-Guzmán, A. Belmonte, J. Torres, T. Neely, M. Baker, R. Gordon, A. Stilgoe, J. Romero, A. G. White, R. Fickler, A. Willner, G. Xie, B. McMorran, and A. Weiner, "Roadmap on structured light," *J. Opt.* **19**, 013001 (2017).
5. N. Radwell, R. D. Hawley, J. B. Götte, and S. Franke-Arnold, "Achromatic vector vortex beams from a glass cone," *Nat. Commun.* **7**, 10564 (2016).
6. B. Ndagano, B. Perez-Garcia, F. S. Roux, M. McLaren, C. Rosales-Guzmán, Y. Zhang, O. Mouane, R. I. Hernandez-Aranda, T. Konrad, and A. Forbes, "Characterizing quantum channels with non-separable states of classical light," *Nat. Phys.* **13**, 397–402 (2017).
7. N. A. Rubin, G. D'Aversa, P. Chevalier, Z. Shi, W. T. Chen, and F. Capasso, "Matrix Fourier optics enables a compact full-Stokes polarization camera," *Science* **364**, 106849 (2019).
8. V. Curcio, L. A. Alemán-Castañeda, T. G. Brown, S. Brasselet, and M. A. Alonso, "Birefringent Fourier filtering for single molecule coordinate and height super-resolution imaging with dithering and orientation," *Nat. Commun.* **11**, 5307 (2020).
9. C. Rosales-Guzmán, B. Ndagano, and A. Forbes, "A review of complex vector light fields and their applications," *J. Opt.* **20**, 123001 (2018).
10. J. Wang, F. Castellucci, and S. Franke-Arnold, "Vectorial light-matter interaction: exploring spatially structured complex light fields," *AVS Quantum Sci.* **2**, 031702 (2020).
11. R. M. A. Azzam, "Stokes-vector and Mueller-matrix polarimetry [invited]," *J. Opt. Soc. Am. A* **33**, 1396–1408 (2016).
12. J. S. Tyo, D. L. Goldstein, D. B. Chenault, and J. A. Shaw, "Review of passive imaging polarimetry for remote sensing applications," *Appl. Opt.* **45**, 5453–5469 (2006).
13. N. Ghosh, "Tissue polarimetry: concepts, challenges, applications, and outlook," *J. Biomed. Opt.* **16**, 110801 (2011).
14. T. Novikova, I. Meglinski, J. C. Ramella-Roman, and V. V. Tuchin, "Polarized light for biomedical applications," *J. Biomed. Opt.* **21**, 71001 (2016).
15. M. Eshaghi and A. Dogariu, "Single-shot omnidirectional Stokes polarimetry," *Opt. Lett.* **45**, 4340–4343 (2020).
16. T. Mu, C. Zhang, and R. Liang, "Demonstration of a snapshot full-Stokes division-of-aperture imaging polarimeter using Wollaston prism array," *J. Opt.* **17**, 125708 (2015).
17. D. N. Naik, R. K. Singh, H. Itou, M. M. Brundavanam, Y. Miyamoto, and M. Takeda, "Single-shot full-field interferometric polarimeter with an integrated calibration scheme," *Opt. Lett.* **37**, 3282–3284 (2012).
18. R. M. A. Azzam, I. M. Elminyaw, and A. M. El-Saba, "General analysis and optimization of the four-detector photopolarimeter," *J. Opt. Soc. Am. A* **5**, 681–689 (1988).
19. J. Ellis and A. Dogariu, "Complex degree of mutual polarization," *Opt. Lett.* **29**, 536–538 (2004).
20. D. S. Sabatke, E. L. Dereniak, G. S. Phipps, M. R. Descour, S. A. Kemme, and W. C. Sweatt, "Optimization of retardance for a complete Stokes polarimeter," *Opt. Lett.* **25**, 802–804 (2000).
21. J. S. Tyo, "Design of optimal polarimeters: maximization of signal-to-noise ratio and minimization of systematic error," *Appl. Opt.* **41**, 619–630 (2002).
22. C. He, H. He, H. Ma, J. Chang, N. Zeng, R. Liao, and Y. Wang, "Linear polarization optimized Stokes polarimeter based on four-quadrant detector," *Appl. Opt.* **54**, 4458–4463 (2015).
23. J. Chang, H. He, Y. Wang, Y. Huang, X. Li, C. He, R. Liao, N. Zeng, S. Liu, and H. Ma, "Division of focal plane polarimeter-based 3×4 Mueller matrix microscope: a potential tool for quick diagnosis of human carcinoma tissues," *J. Biomed. Opt.* **21**, 056002 (2016).
24. C. He, J. Chang, Q. Hu, J. Wang, J. Antonello, H. He, S. Liu, J. Lin, B. Dai, D. S. Elson, P. Xi, H. Ma, and M. J. Booth, "Complex vectorial optics through gradient index lens cascades," *Nat. Commun.* **10**, 1 (2019).
25. X. Li, H. Li, Y. Lin, J. Guo, J. Yang, H. Yue, K. Li, C. Li, Z. Cheng, H. Hu, and T. Liu, "Learning-based denoising for polarimetric images," *Opt. Express* **28**, 16309–16321 (2020).
26. A. Abubakar, X. Zhao, M. Takruri, E. Bastaki, and A. Bermak, "A hybrid denoising algorithm of BM3D and KSVD for Gaussian noise in DoFP polarization images," *IEEE Access* **8**, 57451–57459 (2020).
27. J. M. Bueno, "Polarimetry using liquid-crystal variable retarders: theory and calibration," *J. Opt. A* **2**, 216 (2000).
28. O. Arteaga, J. Freudenthal, B. Wang, and B. Kahr, "Mueller matrix polarimetry with four photoelastic modulators: theory and calibration," *Appl. Opt.* **51**, 6805–6817 (2012).
29. A. Skumanich, B. W. Lites, V. M. Pilet, and P. Seagraves, "The calibration of the advanced Stokes polarimeter," *Astrophys. J. Suppl. Ser.* **110**, 357–380 (1997).
30. M. H. Smith, M. A. Miller, R. V. Blumer, M. A. Stevens, D. M. Teale, and J. D. Howe, "Infrared Stokes polarimeter calibration," *Proc. SPIE* **4133**, 55–64 (2000).
31. C. He, H. He, J. Chang, B. Chen, H. Ma, and M. J. Booth, "Polarisation optics for biomedical and clinical applications: a review," *Light Sci. Appl.* **10**, 194 (2021).
32. M. R. Foreman and F. Goudail, "On the equivalence of optimization metrics in Stokes polarimetry," *Opt. Eng.* **58**, 082410 (2019).
33. A. Vella and M. A. Alonso, "Optimal birefringence distributions for imaging polarimetry," *Opt. Express* **27**, 36799–36814 (2019).
34. V. Shvedov, W. Krolikowski, W. She, and W. Zhu, "Transverse spin angular momentum of tightly focused full Poincaré beams," *Opt. Express* **23**, 34029–34041 (2015).
35. C. He, M. Booth, and M. Booth, "Extraordinary beam modulation with ordinary GRIN lenses," *Opt. Photonics News* **31**, 47 (2020).
36. L.-G. Wang, "Optical forces on submicron particles induced by full Poincaré beams," *Opt. Express* **20**, 20814–20826 (2012).
37. G. Piquero, L. Monroy, M. Santarsiero, M. Alonzo, and J. C. G. D. Sande, "Synthesis of full Poincaré beams by means of uniaxial crystals," *J. Opt.* **20**, 065602 (2018).
38. Q. Zhan, W. Han, and W. Cheng, "Flat-top focusing with full Poincaré beams under low numerical aperture illumination," *Opt. Lett.* **36**, 1605–1607 (2011).
39. A. M. Beckley, M. A. Alonso, and T. G. Brown, "Full Poincaré beams," *Opt. Express* **18**, 10777–10785 (2010).

40. A. A. Galabada Dewage and T. G. Brown, "Interferometric polarimetry using full-Poincare beams," *Proc. SPIE* **11701**, 117010N (2021).
41. A. M. Beckley and T. G. Brown, "Pupil polarimetry using stress-engineered optical elements," *Proc. SPIE* **7570**, 757011 (2010).
42. S. Sivankutty, E. R. Andresen, G. Bouwmans, T. G. Brown, M. A. Alonso, and H. Rigneault, "Single-shot polarimetry imaging of multicore fiber," *Opt. Lett.* **41**, 2105–2108 (2016).
43. R. D. Ramkhalawon, T. G. Brown, and M. A. Alonso, "Imaging the polarization of a light field," *Opt. Express* **21**, 4106–4115 (2013).
44. J. Chang, H. He, C. He, Y. Wang, N. Zeng, R. Liao, and H. Ma, "Optimization of GRIN lens Stokes polarimeter," *Appl. Opt.* **54**, 7424–7432 (2015).
45. J. Chang, N. Zeng, H. He, Y. He, and H. Ma, "Single-shot spatially modulated Stokes polarimeter based on a GRIN lens," *Opt. Lett.* **39**, 2656–2659 (2014).
46. F. Gori, "Measuring Stokes parameters by means of a polarization grating," *Opt. Lett.* **24**, 584–586 (1999).
47. B. G. Zimmerman, T. G. Brown, P. Yang, H. Wei, G. W. Kattawar, Y. X. Hu, D. M. Winker, C. A. Hostetler, and B. A. Baum, "Star test image-sampling polarimeter," *Opt. Express* **24**, 23154–23161 (2016).
48. R. Ramkhalawon, A. M. Beckley, and T. G. Brown, "Star test polarimetry using stress-engineered optical elements," *Proc. SPIE* **8227**, 82270Q (2012).
49. A. Krizhevsky, I. Sutskever, and G. E. Hinton, "ImageNet classification with deep convolutional neural networks," *Commun. ACM* **60**, 84–90 (2017).
50. K. He, X. Zhang, S. Ren, and J. Sun, "Deep residual learning for image recognition," in *IEEE Conference on Computer Vision and Pattern Recognition (CVPR)* (2016), pp. 770–778.
51. R. Szeliski, *Computer Vision: Algorithms and Applications* (Springer, 2010).
52. C. Steger, M. Ulrich, and C. Wiedemann, *Machine Vision Algorithms and Applications* (Wiley-VCH, 2018).
53. T. von Eicken, A. Basu, V. Buch, and W. Vogels, "U-Net: a user-level network interface for parallel and distributed computing," *ACM SIGOPS Operat. Syst. Rev.* **29**, 40–53 (1995).
54. M. Jung, S. Dutta-Gupta, N. Dabidian, I. Brener, M. Shcherbakov, and G. Shvets, "Polarimetry using graphene-integrated anisotropic metasurfaces," *ACS Photonics* **5**, 4283–4288 (2018).
55. A. Espinosa-Soria, F. J. Rodríguez-Fortuño, A. Griol, and A. Martínez, "On-chip optimal Stokes nanopolarimetry based on spin-orbit interaction of light," *Nano Lett.* **17**, 3139–3144 (2017).
56. F. Capasso, J. P. B. Mueller, and K. Leosson, "Ultracompact metasurface in-line polarimeter," *Optica* **3**, 42–47 (2016).
57. A. Pors, M. G. Nielsen, and S. I. Bozhevolnyi, "Plasmonic metagratings for simultaneous determination of Stokes parameters," *Optica* **2**, 716–723 (2015).
58. A. Basiri, X. Chen, J. Bai, P. Amrollahi, J. Carpenter, Z. Holman, C. Wang, and Y. Yao, "Nature-inspired chiral metasurfaces for circular polarization detection and full-Stokes polarimetric measurements," *Light Sci. Appl.* **8**, 78 (2019).